CrystEngComm

PAPER

View Article Online
View Journal | View Issue

Cite this: *CrystEngComm*, 2015, **17**, 1453

Synthesis and aggregation properties of a series of dumbbell polyhedral oligosilsesquioxane-perylene diimide triads†

Ying Zhang,[a] Liangliang Zhang,[b] Heyuan Liu,[a] Di Sun[a] and Xiyou Li*[a]

A series of perylenetetracarboxylic diimide (PDI) derivatives connected with two bulky polyhedral oligosilsesquioxanes (POSSs) were designed and synthesized for the purpose of revealing the effect of bulky and well-defined side groups on the self-aggregation behaviour of PDIs. The properties of these compounds in solution were investigated by UV-vis absorption spectroscopy, fluorescence spectroscopy, and fluorescence quantum yield measurement. The results indicate that the POSS groups do not show large effects on the spectroscopic properties of PDIs in solution. However, the solid state spectroscopic properties of these compounds are significantly affected by the bulky POSS groups. The presence of bulky POSS groups changes the packing structure of the molecules in the solid state and thus affects the solid state emission properties. Our results revealed that the introduction of bulky POSS groups into the molecules will not inevitably lead to promoted solid state fluorescence quantum yield as expected. It is the packing structure of the molecules in the solid state which determines the solid state fluorescence quantum yield. If the presence of bulky POSS groups leads to the formation of "J" aggregates in the solid state, then the solid state fluorescence quantum yields will be improved significantly. Otherwise, if the bulky POSS groups cause "H" type aggregation of the molecules, the solid state fluorescence quantum yields will be small.

Received 3rd December 2014,
Accepted 2nd January 2015

DOI: 10.1039/c4ce02392g

www.rsc.org/crystengcomm

Introduction

Perylenetetracarboxylic diimide (PDI) derivatives are a group of important organic dyes because of their various applications, such as organic field-effect transistors,[1–3] light emitting diodes,[4–11] and solar cells.[12–14] PDIs are well known for their excellent photochemical and thermal stabilities and high fluorescence quantum yields. But the varied applications of PDI in different fields require different photophysical or chemical properties, which can be achieved by introducing different substituents at different positions of PDI molecules.

The substitution positions of PDI molecules can be divided into three categories. They are the imide *N*,*N*′ positions, the 1, 6, 7, 12 positions of the hydrocarbon core (the "bay" positions)[15] and the 2, 5, 8, 11 positions (the peripheral positions). The substituents at imide nitrogen atoms normally lead to significant improvement in solubility in conventional organic solvents. Normally, no significant change in the photophysical properties can be observed with substitution at the imide position of PDIs due to the nodes in both HOMO and LUMO along the long axis.[16,17] However, the substitution at the bay positions can change the photophysical properties of PDI significantly by disturbing the plane conformation of the PDI core or the frontier molecular orbital distribution on the molecule skeleton.[18,19] By changing the properties of the bay substituents, the absorption and fluorescence bands can be moved from the visible region to the near infrared region.[20] The peripheral substitution can improve the solubility of molecules in organic solvents and change the photophysical properties simultaneously without disturbing the planar configuration of the PDI core. A recent report reveals efficient singlet fission in the crystal of a peripheral substituted PDI compound.[21] Among the numerous studies on the synthesis of new PDI compounds, reducing the exciton interactions by introducing different groups at different positions and thus increasing the fluorescence quantum yields in the solid state became a very important part, because of the great application potential of these materials. Langhals and coworkers showed that the aggregation of PDI can be prevented by introducing steric inhibiting alkyl groups at the imide nitrogen atoms, and the resulted compound exhibits strong fluorescence in the solid state.[22,23] Liu *et al.*

[a] *Key Laboratory of Colloid and Interface Chemistry of Ministry of Education, Department of Chemistry, Shandong University, Shanda Nan Lu 27#, Jinan, Shandong, 250100, China. E-mail: xiyouli@sdu.edu.cn; Fax: +86 531 88564464*
[b] *Department of Chemistry, College of Science (East China), China University of Petroleum, Qingdao, 266580, China*

† Electronic supplementary information (ESI) available. CCDC 1022045, 1021968, and 1021969. For ESI and crystallographic data in CIF or other electronic format see DOI: 10.1039/c4ce02392g

successfully introduced β-cyclodextrin grafts into the imide *N*, *N*′ positions. This compound exhibits strong solid-state fluorescence and can probe the vapor of organic amines with high sensitivity.[24] Previous studies by our group have shown that the steric hindrance introduced by the substituents at bay positions affects the aggregation behavior of PDI molecules efficiently.[25] Water-soluble PDIs have been obtained by incorporating hydrophilic moieties, including polyglycerol dendrons[26] and Newkome dendrons,[27] to the imide *N*,*N*′ positions, and PDI aggregation could be suppressed and fluorescence quantum yields could be improved in water.[26]

Polyhedral oligosilsesquioxane (POSS) molecules, with a unique nanoscale cage-shaped structure, have been widely incorporated into polymers because of their excellent performance in tuning mechanical strength,[28] thermal stability,[29] and other physical characteristics.[28] Moreover, many POSS-based organic dyes, such as boron dipyrromethene (BODIPY),[30,31] porphyrin,[32] phthalocyanines,[33] and azobenzene compounds,[34] were prepared and showed some new superior properties, such as the reduced aggregation ability in solutions,[32] improved photochemical stabilities[35] and so on. POSS-containing PDI was also prepared, and showed high sensitivity in rapid detection of fluoride ions in aqueous solution.[36] In the present work, we designed and synthesized a series of POSS-containing compounds with different substituents at the bay positions. The structures of these compounds are summarized in Scheme 1. This research aims to reveal the synergistic effect of substituents at the bay positions and POSS groups at the imide nitrogen atoms on the reduction of the aggregation of PDI molecules in the solid state.

Experimental section

Instruments and methods

^{1}H spectra were recorded on a Bruker 300 or 400 MHz NMR spectrometer with chemical shifts reported in ppm (TMS as the internal standard). MALDI-TOF mass spectra were recorded with a Bruker Ultraflex instrument. Absorption spectra were measured on a SHIMADZU UV-2450 spectrophotometer with a wavelength resolution of 0.3 nm. Steady state fluorescence spectra and fluorescence lifetimes were measured on an FLS920 (Edinburgh) fluorometer with excitation at 400 nm. Steady state fluorescence spectra were recorded by exciting the samples with a Xe lamp. The wavelength resolution of the monochromator is 0.1 nm. The fluorescence lifetime data were recorded following 445 nm excitation with a picosecond pulsed laser diode (EPL-445, Edinburgh Instruments). The fluorescence lifetimes were measured by time correlated single photon counting (TSPC). Solution fluorescence quantum yields were calculated with **1a** (100%, 5×10^{-6} M in chloroform) as the standard. The absolute solid state fluorescence quantum yields were measured with integrating spheres on FLS920. Single-crystal X-ray diffraction data of **3b** and **3c** were collected with the use of an Agilent Xcalibur Eos Gemini diffractometer with an Enhance (Cu) X-ray source (Cu-Kα, λ = 1.54178 Å). The data were collected at 150 K because the crystals lose the solvent quickly and have extensive disorder in the solvent sphere. Single-crystal X-ray diffraction data of **1b** were collected at room temperature. All absorption corrections were applied using the multiscan program SADABS. All structures were solved by direct methods using the SHELXS-97[37] program of the SHELXTL package and refined by the full-matrix least-squares method with SHELXL-97.[38]

The thin solid films of these compounds were prepared by dropping the solution of the compounds in chloroform to the cleaned surface of quartz (for spectroscopy measurements) and crystal silica (for XRD experiments). Single crystals suitable for X-ray diffraction were obtained by dissolving **1b** in $CHCl_3$, and **3b** and **3c** in a mixture of $CHCl_3$/MeOH = 3 : 2, followed by slow evaporation of the solvents.

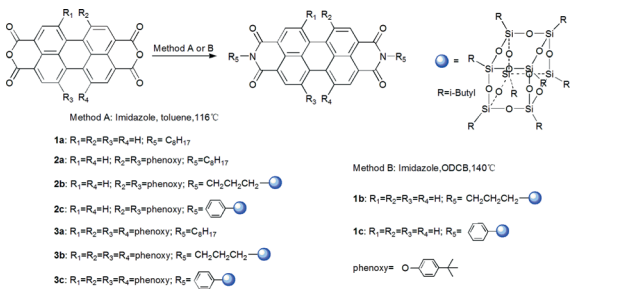

Scheme 1 Synthetic and molecular structures of compounds **1a–c**, **2a–c**, and **3a–c**.

Materials

Aminopropylisobutyl POSS (AM0265) and *p*-aminophenylisobutyl POSS (AM0292) were purchased from Hybrid Plastics. Imidazole and *o*-dichlorobenzene (ODCB) were purchased from J&K. Perylene-3,4,9,10-tetracarboxylic dianhydride and other chemicals were purchased from commercial sources. Solvents were of analytical grade and used directly without any purification. **1a**[39] and **1c**[40] were prepared according to the literature. **1b**, **2a–c**, and **3a–c** were synthesized by either method A or method B.

Method A. Perylene-3,4,9,10-tetracarboxylic dianhydride (0.05 mmol), amines (0.15 mmol) and imidazole (0.5 g) in toluene (15 ml) were heated to reflux under a nitrogen atmosphere and kept at reflux for 24 h.[41] The solvent was removed under reduced pressure and the residue was washed with dilute hydrochloric acid (10%, 100 mL) and then water. The product was purified by column chromatography on silica gel (200–300 mesh). After recrystallization from chloroform and methanol, the product was collected and subjected to structure characterization.

Method B. Perylene-3,4,9,10-tetracarboxylic dianhydride (0.05 mmol), *p*-aminophenylisobutyl POSS (0.15 mmol), imidazole (0.5 g), and 2 mL of *o*-dichlorobenzene (ODCB) were refluxed at 140 °C under nitrogen atmosphere for 6 h. After cooling, the reaction mixture was dispersed in 20 mL of ethanol and 20 mL of HCl (2 N). The mixture was extracted two

times with 200 mL of chloroform. The combined organic phase was washed with 5% $NaHCO_3$ aqueous solution until neutral, then it was concentrated and purified by column chromatography on silica gel (200–300 mesh). After recrystallization from chloroform and methanol, the product was subjected to structure characterization.

1a: Method A. The product was purified by column chromatography with chloroform as the eluent, and collected as a dark red solid with a yield of 90%. ^{1}H NMR ($CDCl_3$, 300 MHz, ppm): δ 8.67 (m, 8H), 4.22 (t, 4H), 1.79 (m, 4H), 1.29 (m, 20H), 0.89 (t, 6H). Anal. calcd for $C_{40}H_{42}N_2O_4$ (%): C 78.15, H 6.89, N 4.56; found: C 78.37, H 6.67, N 4.42.

1b: Method B. The product was purified by column chromatography with chloroform as the eluent; **1b** was collected as a red solid with a yield of 88%. ^{1}H NMR ($CDCl_3$, 300 MHz, ppm): δ 8.68 (m, 8H), 4.21 (m, 4H), 1.84 (m, 18H), 0.94 (m, 84H), 0.74 (t, 4H), 0.58 (m, 28H). MALDI-TOF (*m*/*z*): calcd 2102.64; found 2125.720 [M + Na^+]; anal. calcd for $C_{86}H_{146}N_2O_{28}Si_{16}$ (%): C 48.99, H 7.12, N 1.28; found: C 49.06, H 6.99, N 1.33.

1c: Method B. Yield 43%. ^{1}H NMR ($CDCl_3$, 300 MHz, ppm): δ 8.76 (m, 8H), 7.87 (d, 4H), 7.37 (d, 4H), 1.91 (m, 14H), 0.98 (m, 84H), 0.66 (m, 28H). Anal. calcd for $C_{92}H_{142}N_2O_{28}Si_{16}$ (%): C 50.84, H 6.59, N 1.29; found: C 50.59, H 6.74, N 1.21.

2a: Method A. The mixture was purified by column chromatography with dichloromethane/hexane (v/v = 5 : 4) as the eluent, and **2a** was collected with a yield of 77%. ^{1}H NMR ($CDCl_3$, 300 MHz, ppm): δ 9.61 (d, 2H), 8.59 (d, 2H), 8.36 (s, 2H), 7.47 (t, 4H), 7.10 (t, 4H), 4.14 (t, 4H), 1.75 (m, 4H), 1.37 (s, 18H), 1.25 (m, 20H), 0.86 (m, 6H). ^{13}C NMR ($CDCl_3$, 75 MHz, ppm): 162.2, 161.8, 154.4, 151.5, 147.2, 132.3, 129.0, 128.1, 127.7, 126.4, 123.8, 122.7, 122.6, 121.1, 118.1, 39.6, 33.5, 30.8, 30.4, 28.3, 28.2, 27.0, 26.1, 21.6, 13.1; MALDI-TOF (*m*/*z*): calcd 910.49; found 910.99 [M^+]. Anal. calcd for $C_{60}H_{66}N_2O_6$ (%): C 79.09, H 7.30, N 3.07; found: C 78.92, H 7.47, N 3.14.

2b: Method A. The mixture was purified by column chromatography with chloroform/hexane (v/v = 4 : 1) as the eluent to give compound **2b** in 45% yield. ^{1}H NMR ($CDCl_3$, 300 MHz, ppm): 9.63 (m, 2H), 8.60 (m, 2H), 8.37 (s, 2H), 7.45 (t, 4H), 7.10 (t, 4H), 4.14 (m, 4H), 1.82 (m, 18H), 1.50 (s, 4H), 1.36 (s, 18H), 0.91 (m, 84H), 0.58 (m, 28H). ^{13}C NMR ($CDCl_3$, 75 MHz, ppm): 163.3, 162.9, 155.5, 152.7, 148.1, 133.5, 130.1, 129.4, 128.8, 127.4, 125.1, 123.9, 123.8, 122.3, 119.1, 42.9, 34.5, 31.5, 25.7, 23.84, 22.4, 21.5, 9.8; MALDI-TOF (*m*/*z*): calcd 2398.81; found 2400.15 [M + H^+]. Anal. calcd for $C_{106}H_{170}N_2O_{30}Si_{16}$ (%): C 53.01, H 7.13, N 1.17; found: C 52.87, H 7.24, N 1.07.

2c: Method B. The product was purified by column chromatography using hexane/dichloromethane (v/v = 3 : 2) as the eluent. The product was collected with a yield of 61%. ^{1}H NMR ($CDCl_3$, 300 MHz, ppm): δ 9.64 (d, 2H), 8.60 (d, 2H), 8.40 (s, 2H), 7.82 (m, 4H), 7.46 (m, 4H), 7.32 (d, 4H), 7.12 (m, 4H), 1.50 (s, 4H), 1.36 (s, 18H), 0.91 (m, 84H), 0.58 (m, 28H). ^{13}C NMR ($CDCl_3$, 75 MHz, ppm): 163.7, 163.4, 156.1, 152.7, 148.7, 137.0, 135.4, 134.2, 133.2, 130.8, 129.9, 129.3, 128.0, 127.8, 125.6, 124.3, 124.1, 122.6, 119.6, 34.6, 31.5, 29.7, 25.7, 23.9, 22.6; MALDI-TOF (*m*/*z*): calcd 2466.78; found 2467.39 [M + H^+]. Anal. calcd for $C_{112}H_{166}N_2O_{30}Si_{16}$ (%): C 54.46, H 6.77, N 1.13; found: C 54.03, H 6.59, N 1.01.

3a: Method A. The mixture was purified by column chromatography with dichloromethane/hexane (v/v = 3 : 2) as the eluent, and obtained as a dark red solid in 56% yield. ^{1}H NMR ($CDCl_3$, 300 MHz, ppm): δ 8.22 (s, 4H), 7.22–7.25 (m, 8H), 6.80–6.84 (m, 8H), 4.08–4.12 (t, 4H), 1.62–1.69 (m, 4H), 1.23–1.29 (m, 56H), 0.83–0.86 (t, 6H). ^{13}C NMR ($CDCl_3$, 75 MHz, ppm): 163.3, 155.9, 152.9, 147.3, 132.9, 126.6, 122.5, 120.4, 119.9, 119.5, 119.3, 42.9, 34.4, 31.5, 25.69, 25.67, 23.8, 22.5, 22.4, 21.6, 9.75; MALDI-TOF (*m*/*z*): calcd 1206.67; found 1207.93 [M + H^+]. Anal. calcd for $C_{80}H_{90}N_2O_8$ (%): C 79.57, H 7.51, N 2.32; found: C 79.35, H 7.67, N 2.17.

3b: Method A. The resulting product was purified by column chromatography with dichloromethane/hexane (v/v = 3 : 2) as the eluent, and collected as a red solid with a yield of 45%. ^{1}H NMR ($CDCl_3$, 300 MHz, ppm): δ 8.14 (s, 4H), 7.22 (m, 8H), 6.82 (m, 8H), 4.09 (t, 4H), 1.81 (m, 18H), 1.29 (s, 36H), 0.91 (m, 84H), 0.56 (m, 32H); ^{13}C NMR ($CDCl_3$, 75 MHz, ppm): 162.4, 154.9, 151.9, 146.2, 131.9, 125.6, 121.5, 119.5, 118.8, 118.4, 118.3, 39.6, 33.3, 30.7, 30.4, 28.2, 26.1, 21.6, 13.0; MALDI-TOF (*m*/*z*): calcd 2694.99; found 2695.57 [M + H^+]. Anal. calcd for $C_{126}H_{194}N_2O_{32}Si_{16}$ (%): C 56.09, H 7.25, N 1.04; found: C 55.78, H 7.37, N 1.11.

3c: Method A. The desired product was further purified by column chromatography using hexane/dichloromethane (v/v = 3 : 2) as the eluent to get compound **3c** in 48% yield. ^{1}H NMR ($CDCl_3$, 400 MHz, ppm): δ 8.27 (s, 4H), 7.79 (d, 4H), 7.25 (d, 12H), 6.87 (d, 8H), 1.88 (m, 14H), 1.29 (s, 36H), 0.95–0.99 (m, 84H), 0.64–0.66 (m, 28H). ^{13}C NMR ($CDCl_3$, 75 MHz, ppm): 163.7, 156.1, 152.8, 147.4, 137.0, 135.0, 133.2, 132.7, 127.7, 126.7, 122.6, 120.7, 120.2, 119.8, 119.4, 34.4, 31.41, 25.7, 23.9, 22.5. MALDI-TOF (*m*/*z*): calcd 2762.96; found 2762.70 [M^+]. Anal. calcd for $C_{132}H_{190}N_2O_{32}Si_{16}$ (%): C 57.31, H 6.92, N 1.01; found: C 56.56, H 7.03, N 0.92.

Results and discussion

Molecular design and synthesis

The effects of bulky substituents and branched alkyl tails on the modification of phase structures and molecular packing have been nicely illustrated by previous studies.[42,43] Polyhedral oligosilsesquioxanes (POSSs), regarded as small inorganic nanoparticles with diameters up to 1.5 nm,[44] were chosen as the bulky group because of their well-defined nature. The incorporation of POSS into organic molecules can bring remarkable improvement in the thermal and oxidative stability.[45] More importantly, the highly crystalline packing of POSS cages can sometimes aid the self-assembly in forming ordered structures in the solid state. Nevertheless, there are few reports on the systematic study of the effect of POSS on the self-assembly and ordered packing of π-conjugated materials[32] in the solid state. Therefore, POSS was chosen as a structural motif to couple with PDI as a model system to

examine the effect of bulky groups at the imide nitrogen atoms and bay positions on the self-assembly of PDIs.

There are basically two ways to link POSS to both nitrogen atoms of PDI: through a rigid linkage or a flexible linkage. The former gives shape-persistent dumbbell-like molecules, while the latter gives relatively flexible molecules. If the flexible linkage between POSS and PDI is used, the interaction between POSS and PDI will be small, and therefore, less influence is expected for the POSS on the self-assembly of PDIs.[46] Therefore, the POSS cages are covalently attached to PDI through both a flexible linkage and a rigid linkage.

The general synthetic procedures are shown in Scheme 1. All the new compounds were prepared by the coupling of 3,4,9,10-perylenetetracarboxylic dianhydride (PDA), 1,7-di(*p-tert*-butylphenoxy)perylene-3,4,9,10-tetracarboxylic dianhydride, and 1,6,7,12-tetra(*p-tert*-butylphenoxy)perylene-3,4,9,10-tetracarboxylic dianhydride with the corresponding amino POSS. Two different methods are employed in the preparation of these compounds: method A (refluxing in imidazole/toluene) and method B (refluxing in imidazole/ODCB). Compounds **1a**, **2a–b**, and **3a–b** were prepared with method A and the rest of the compounds were prepared with method B. For the PDAs without substituents at the bay positions, the coupling between the dianhydride and the amino-POSS was easier in imidazole/ODCB with higher production yields. Otherwise, for the PDA with bay position substitutions, the coupling will be easier in imidazole/toluene because of the improved solubility of PDAs. The molecular structure of these new compounds has been fully characterized by ^{1}H NMR, MALDI-TOF mass and elemental analysis.

Properties of these compounds in solution

The optical properties of these new compounds in solution were investigated by UV-vis and fluorescence spectroscopy. The spectra of **2a–c** and **3a–c** are shown in the ESI† (Fig. S1).

Fig. 1 shows the absorption and emission spectra of **1a–c** in $CHCl_3$. All these three compounds (**1a–c**) exist as isolated molecules and no aggregate was found in the solution, as revealed by the absorption spectra.[47] In the visible region, three pronounced absorption bands are observed at 457 nm, 488 nm, and 525 nm for **1a**. The band at 525 nm represents the lowest energy transition from the ground state to the first excited state, whilst the subsequent maxima at 488 and 457 nm correspond to transitions to various excited vibrational levels of the first electronic excited state, consistent with the previous findings.[48–50] The absorption spectra of **1b** are identical to that of **1a**, and no difference in the maximum absorption wavelength and molar extinction coefficient can be identified, which means that the POSS groups linked by the flexible linkage at the imide nitrogen atoms do not interact with the PDI core. The absorption spectra of **1c** are also very similar with those of **1a** and **1b**, but a small red-shift (about 2 nm) of the absorption maximum can be identified. It is not a system error caused by the instrument, because on the one hand the wavelength resolution of the instrument

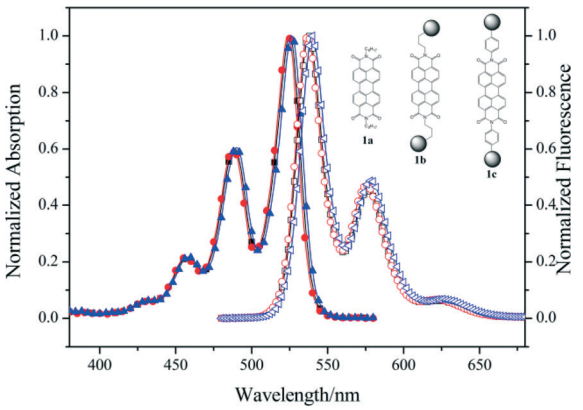

Fig. 1 UV-vis absorption (solid) and fluorescence spectra (hollow) of **1a** (black square), **1b** (red circle), and **1c** (blue triangle) in chloroform (5.0×10^{-6} M) at room temperature. The inset shows the molecular structures of **1a–c**.

(0.3 nm) is much smaller than the shift, and on the other hand similar red-shifts have been found for **2c** and **3c** in comparison with their counterparts **2a** and **3a**, respectively. This means, despite the molecular orbital knots on the imide nitrogen atoms, that the phenyl bridge has indeed influenced the absorption spectrum of PDI slightly.

By comparing the absorption spectra of **2a–c** and **3a–c** (Fig. S1(a, b) ESI†) with those of **1a–c**, we can find that the introduction of phenoxyl groups at the bay position has caused a significant red-shift of the maximum absorption peak, which can be attributed to the electron-donating nature of the *p-tert*-butylphenoxy groups and can be explained by König's color theory.[51,52] It should also be noted that the cleanly resolved progression of the vibrational peaks observed in the absorption spectra of **1a–c** is nearly lost in those of **2a–c** and **3a–c**. The band broadening observed can be attributed to two reasons. One could be the increase of the conjugation between the substituents and the perylene core.[53,54] Another could be the twisting of the PDI core by the substituent.[55,56]

The fluorescence emission spectrum of compound **1a**, with a maximum at λ_{max} = 537 nm, is a mirror image of the S_0–S_1 absorption band. Fluorescence emission spectra identical to that of **1a** have been recorded for **1b**, indicating no interaction between POSS and PDI core in compound **1b**. A small red-shift can be identified for the fluorescence emission maximum of **1c** compared with that of **1a**, suggesting the weak interactions between the phenyl bridge and the PDI core in compound **1c**, which is consistent with the results of absorption spectra. The Stokes shift of **1a** is 12 nm, which increased to 33 nm and 35 nm for **2a** and **3a**, respectively, owing to a pronounced vibronic progression and conformational disorder imparted by the core-twisted chromophores.[57]

Besides the absorption and emission spectra, the fluorescence quantum yields and fluorescence lifetimes are also measured for these compounds and the results are summarized in Table 1. The fluorescence intensity of all these compounds decays mono-exponentially and only one fluorescence

Table 1 UV and fluorescence spectroscopic parameters of **1a–c**, **2a–c** and **3a–c** in $CHCl_3$ (5×10^{-6} M)

	λ_{abs}[a]/nm	ε[b]	λ_{em}/nm	τ(ns)	χ^2	Φ_f[c]
1a	525	9.3	537	4.28	1.00	1
1b	524	9.1	536	4.30	1.00	1
1c	526	9.5	539	4.01	1.00	0.92
2a	546	5.1	580	5.28	1.00	0.71
2b	545	4.9	579	5.22	1.00	0.71
2c	549	4.9	582	4.84	1.00	0.71
3a	583	5.1	618	6.76	1.01	0.46
3b	581	5.0	615	6.63	1.00	0.47
3c	586	5.2	620	6.19	1.00	0.44

[a] At the absorption maximum. [b] Molar absorption coefficient at the absorption maximum. ε: ($\times 10^4$ L mol^{-1} cm^{-1}). [c] With monomeric **1a** (5.0×10^{-6} M) as reference ($\Phi_f = 1$).

lifetime for each of them can be measured. The fluorescence lifetimes measured for **1a–c** are similar to each other, and the same results can be deduced from the fluorescence lifetimes of **2a–c** and **3a–c**, indicating that no extra photo-induced process within these molecules has been introduced by POSS. The same result is suggested by their similar fluorescence quantum yields.

Aggregation of these compounds in the solid state

The thin solid films of these compounds are prepared by casting a $CHCl_3$ solution of these compounds on the surface of the substrate and then allowing the solvents to evaporate gradually at room temperature. Because UV-vis absorption and fluorescence spectra are sensitive to the inter-chromophore distance and orientation,[58,59] they have been widely used to study the π–π stacking of organic dyes.[60–62] Moreover, a series of PDI dimers and oligomers with rigid molecular structure have been prepared and the absorption spectra have been reported,[41,59,63,64] which provides us with good references to determine the packing structure of the PDI molecules in the solid state by spectroscopy. So the packing structure of the molecules in the solid state was first examined by solid state absorption spectroscopy. All the spectroscopic parameters of these compounds in the solid state are summarized in Table 2 and the spectra are shown in Fig. 2–4.

The absorption spectra of the thin solid films of **1a–c** are shown in Fig. 2. The absorption spectra of **1a** in solution are also shown for the purpose of comparison. In the absorption spectra of **1a** thin solid films, several absorption bands appeared in the region of 400–600 nm, with the maximum

Table 2 Absorption and fluorescence spectroscopic parameters of **1a–c**, **2a–c** and **3a–c** thin solid films

	1a	**1b**	**1c**	**2a**	**2b**	**2c**	**3a**	**3b**	**3c**
λ_{abs}/nm	488	491	498	578	509	561	603	601	594
λ_{em}/nm	690	632	674	671	655	668	638	636	645
Φ_f[a] [%]	2.2	39.0	17.8	13.0	5.1	13.0	14.6	17.5	47.2

[a] Absolute fluorescence quantum yields measured by integrating spheres.

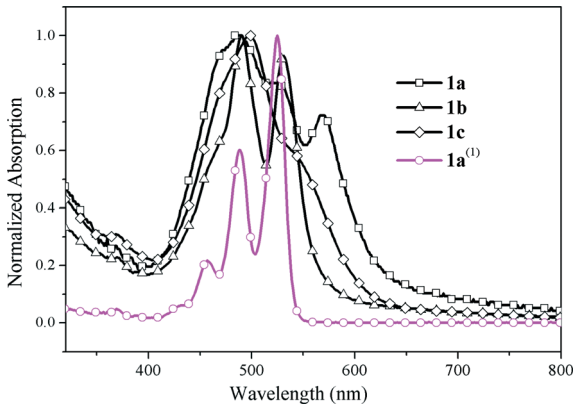

Fig. 2 Normalized absorption spectra of thin films of **1a–c**. (1): With monomeric **1a** (5.0×10^{-6} M in chloroform) as reference.

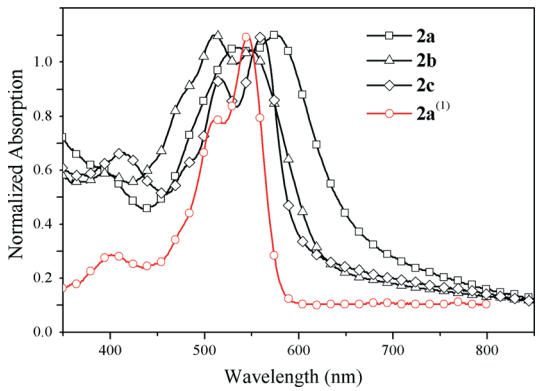

Fig. 3 Normalized absorption spectra of thin films of **2a–c**. (1): With monomeric **2a** (5.0×10^{-6} M in chloroform) as reference.

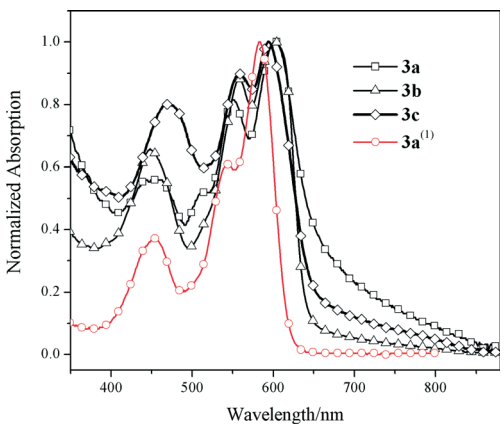

Fig. 4 Normalized absorption spectra of thin films of **3a–c**. (1) With monomeric **3a** (5.0×10^{-6} M in chloroform) as reference.

absorption at around 500 nm. Another small absorption band with a relatively smaller intensity can be found at 570 nm, which red-shifted for about 46 nm in comparison with the 0–0 transition of **1a** in solution. The blue-shifting of the maximum absorption band can be attributed to the "H" type (face-to-face) interaction,[24,65] while the red-shifted absorption band is a sign of the presence of "J" type aggregation (head-to-tail).[57,66] These spectral features of **1a** in

the solid state suggest that there are different relative orientations between the neighbour molecules of **1a**, which cause different changes in the absorption spectra. This is understandable, because there are no substituents at the bay positions and bulky groups at imide nitrogen atoms, the molecules of **1a** can approach each other from different directions and then cause different interactions between the molecules.

In the absorption spectra of **1b** thin solid films shown in Fig. 2, two sharp absorption bands around 491 and 531 nm can be found. These two bands red-shifted slightly with respect to those of **1b** in solution with the one at 491 nm having the largest intensity. Because similar spectral changes (red shift and intensity reverse for the 0–0 and 0–1 vibration bands) have been previously reported for a "face-to-face" stacked PDI dimer with longitudinal displacement,[63] we suggest that the molecules of **1b** in the solid films take similar relative orientations, *i.e.* stacking in a "face-to-face" way, but with longitudinal displacement between the neighbour PDI molecules. The absorption spectra of **1c** thin solid films show a broad absorption band with the maximum absorption at about 499 nm, which blue-shifted for about 34 nm compared with the maximum absorption of **1a** in solution. This is a clear indication of the "face-to-face" stacked structure without large longitudinal displacement, *i.e.* "H" type aggregation.[41]

By comparing the absorption spectra of **1a**, **1b** and **1c** in the solid state, we can conclude that there are different relative orientations between the molecules of **1a** in the solid state, which brings about different spectral changes against their spectra in solution. This may be ascribed to either the different microcrystallines in the solid state of **1a**, or the different relative orientations between the neighbour molecules of **1a** along different directions in the solid state. However, after the POSS are connected by a flexible linkage, the interactions between the molecules of **1b** can be assigned to a slipped "face-to-face" structure with obvious longitudinal displacement. When POSS is linked to the PDI core by rigid linkages, the molecules of **1c** in the solid state take a "face-to-face" stacked structure too, but without significant longitudinal displacement.

The absorption spectra of **2a–c** in the solid state are shown in Fig. 3. The absorption spectra of **2a** in the solid state present two broad and red-shifted absorption bands with respect to its spectra in solution, which indicates the formation of a "face-to-face" stacked structure with large longitudinal displacement.[63] Based on the red-shift of the 0–0 and 0–1 transition absorption bands, we suggest that the molecules of **2a** in the solid state form "J" aggregates.[63] The absorption spectra of **2b** present also broad absorption bands, but the 0–1 vibration band has the largest intensity. This means that the molecules of **2b** formed "H" aggregates in the solid state with small longitudinal displacement.[41] The absorption spectra of **2c** present two red-shifted absorption bands, with the 0–0 transition having the largest absorption intensity. This is a typical absorption pattern of "face-to-face" stacked aggregates with large longitudinal displacement, *i.e.* "J" type aggregates.[57,63,66]

In general, as revealed by the absorption spectra of **2a–c** in the solid state, **2a** and **2c** form a "face-to-face" stacked structure with large longitudinal displacement in the solid state. Because the red-shift of the absorption band of **2c** is smaller than that of **2a**, the interaction between the molecules of **2c** in the solid state is weaker than that of **2a**, probably because of the steric hindrance caused by the bulky POSS groups. **2b** forms "H" type aggregates in the solid state.

The solid state absorption spectra of **3a–c** are collected in Fig. 4. PDIs with four phenoxyl groups have a smaller tendency to form aggregates, because of the steric hindrance caused by the four bulky phenoxy groups at the bay positions.[25,41,57] In solution, they can only form "J" type aggregates with the help of hydrogen bonding or other strong supramolecular driving forces.[57] The solid state absorption spectra of **3a–c** do not show a large difference from that of **3a** in solution except for a small red-shift of the maximum absorption wavelength. The maximum absorption bands of **3a** and **3b** in the solid state are similar. This means that the introduction of POSS by flexible linkage does not bring about large effects on the packing of the molecules in the solid state. The red-shift of the maximum absorption band of **3c** is smaller than that of **3b**, suggesting that the interactions between the molecules of **3c** in the solid state are smaller than those of **3b** and **3a**. This may be ascribed to the rigid linkage between POSS and PDI, which makes the molecules of **3c** more shape-persistent and causes large steric hindrance between the neighbour molecules. Nevertheless, the red-shift of the absorption maximum suggests the formation of "J" type aggregates with a slipped "face-to-face" stacked structure for these three compounds in the solid state. Because of the steric hindrance caused by the bulky POSS at the imide nitrogen and phenoxyl groups at the bay positions, the interactions between the molecules of **3a–c** in the solid state are small.[22,25]

Comparing the packing behaviours of **1a**, **2a** and **3a** in the solid state as revealed by the absorption spectra, we can conclude that without the bay substituents, the PDI molecules can approach a neighbour molecule from different directions and thus lead to different interactions between the molecules. When the bay substituents are introduced, the PDI molecules will prefer to interact with each other from the vertical direction of the PDI plane and form a "face-to-face" stacked structure. The POSS groups linked at the end of the molecules have similar effects to those of the bay substituents, as revealed by the compound series **1a–c**. But the effects of POSS groups on the packing structure of PDI molecules are complicated and change in different molecules. We suggest that it is the result of synergistic effects of bay substituents and imide nitrogen substituents.

The packing structures of these molecules in the solid state are also investigated by single crystal X-ray diffraction experiments. The single crystals are grown from chloroform, the same solvent for the thin solid film preparation; therefore, the crystal structures are good references for the structures of the thin solid films. Because crystals, which are

suitable for single crystal X-ray diffraction experiments, have only been successfully grown for **1b**, **3b** and **3c**, only the crystal structures of these three compounds are measured (for details see the ESI† Table S1). Crystallographic data for the three new crystal structures have been deposited with the Cambridge Crystallographic Data Center as supplementary publication no. CCDC 1022045, 1021968, and 1021969. Minute differences in the crystal structure of **1b** can be found when compared with the reported literature.[67] It is worth noting that the quality of the crystals is poor for all these three compounds, due to the presence of freely rotating groups and solvent molecules. Therefore, the crystal data presented in the CIF files in the ESI† do not meet the usual standard. However, the focus of this research is just the rough packing structure of the PDI cores, which is employed to confirm the results of UV-vis absorption spectra. So the poor crystal diffraction results are still meaningful for this research.

The crystal structure and molecular packing of **1b** are shown in Fig. 5(a and b) and Fig. 6(a and b). Molecules of **1b** crystallized in the triclinic space group $\bar{P}1$. Since POSS groups lie in the same side of the perylene ring, the molecules of **1b** can pack in a "face-to-face" way. The two different views of **1b** reveal that the π-scaffold is planar, the packing arrangement of PDI **1b** is a slipped "face-to-face" structure with longitudinal displacement, and the interplanar distance of two adjacent perylene skeleton planes is 3.61 Å (Fig. 6b), which allows for slight π–π stacking. These are in agreement with the absorption spectra.

Fig. 5c and d show the molecular structure of **3b** as found in the crystal structure. **3b** crystallizes in the space group $\bar{P}1$ with two co-crystallized $CHCl_3$ molecules. The cell contains 4 molecules (Z = 2) in general positions (Fig. 6c and d). The packing arrangement of PDI **3b** is characterized by two slipped stacks of strictly parallel chromophores. The interplanar distance of two adjacent perylene skeleton planes is 3.65 Å, which allows for slight π–π stacking. The two different views of **3b** reveal significant distortion of the π-scaffold (Fig. 5c and d). We divide the perylene scaffold into two naphthalene subunits. The rotational twist of the averaged naphthalene planes with regard to each other is 27.5°, which was taken as the twist angle.[20] Indeed, the core twisting has a significant effect on the molecular packing of **3b**.[68] The "J" type packing of the adjacent **3b** molecules can be seen clearly in Fig. 6d. Besides this "J" type interaction, no other interactions should exist between the molecules of **3b** in the same unit cell or the molecules from other unit cells because of the large distance between them. This is in good agreement with the conclusion deduced from the absorption spectra.

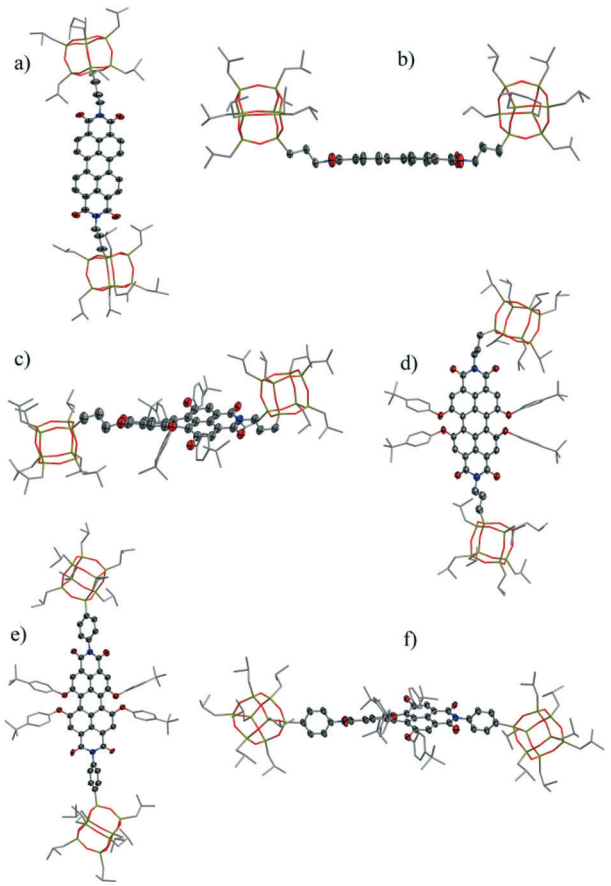

Fig. 5 Molecular structures of **1b** (a and b), **3b** (c and d), and **3c** (e and f) in front view (a, d and e) and side view (b, c, and f). Hydrogen atoms and all solvent molecules were omitted for clarity.

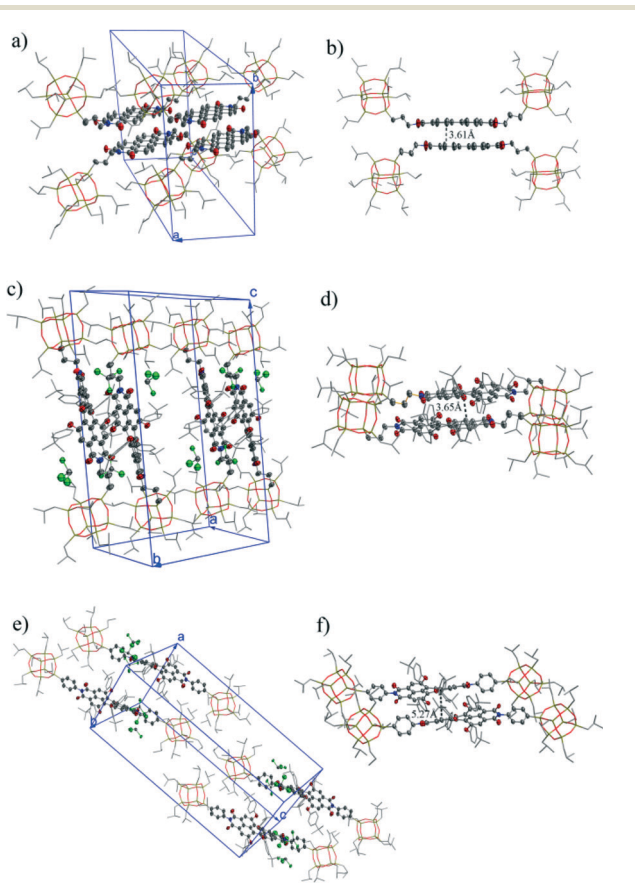

Fig. 6 Molecular packing of solvent-free **1b** (a and b), **3b** co-crystallized with 2 $CHCl_3$ (c and d), and **3c** co-crystallized with 3 $CHCl_3$ (e and f).

Fig. 5(e and f) and 6(e and f) show the molecular structures and molecular packing of **3c**. Single crystal X-ray diffraction analysis also shows that compound **3c** crystallizes in the space group $\bar{P}1$ with three co-crystallized $CHCl_3$ molecules. The cell contains 2 molecules ($Z = 2$) in general positions. The two different views of **3c** (Fig. 5e and f) reveal significant distortion of the π-scaffold. The twist angle between the two naphthalene planes is 27.8(1)°, which is similar to that of **3b**. The packing arrangement of PDI **3c** in the crystal is utterly slipped stack. Although PDI cores have slight π–π intermolecular interactions judged by the distance between the planes of the PDI core, phenoxy groups have electronic interactions with the perylene diimide cores of adjacent molecules. These can have an effect on the molecular packing. Similar to that found for **3b**, the interaction between the adjacent molecules in the crystal of **3c** is limited between two molecules. The interaction should be much weaker because of the large distance between the two PDI cores. The packing structure of **3c** in the crystal corresponds also very well with that revealed by the absorption spectra. It must be noted that the consistency between the single crystal structures of **1b**, **3b** and **3c** and the predicted packing structure from their absorption spectra suggests that the predicted packing structure of other compounds (**1a**, **1c**, **2a–c** and **3a**) based on the absorption spectra should be also reliable.

We have also tried to determine the structure of the thin solid films by low angle X-ray diffraction experiments, but not one of the thin solid films can give any meaningful peaks in the diffraction patterns, which means that the thin solid films prepared by casting chloroform solutions on the substrate do not have a long range order (ESI† Fig. S3).

The solid state emission properties

As mentioned in the introduction part, the introduction of different groups at the imide nitrogen atoms of PDI sometimes leads to strong solid emission,[22] which is much favourable for photonic applications. The bulky POSS as well as the bay substituents can affect the packing structure of the PDI molecules in the solid films, and therefore, they are expected to affect the fluorescence properties significantly too.

The fluorescence properties of the solid films of these compounds are summarized in Table 2. Generally, the fluorescence maxima of the solid films red-shifted dramatically from that in solution, indicating the presence of strong excited state interactions between the neighbour molecules. Compounds **3a–c** present relatively smaller red-shifts of the fluorescence maximum in these three series of compounds, which can be attributed to the reduced interactions among neighbour molecules due to the steric hindrance caused by the four phenoxyl groups attached at the bay positions.

Fig. 7 compares the fluorescence spectra of **1a–c** with that of **1a** in solution. In the fluorescence spectrum of **1a**, two emission bands at about 630 and 700 nm can be identified. These fluorescence bands are roughly the mirror images of the absorption bands shown in Fig. 2 and can be attributed

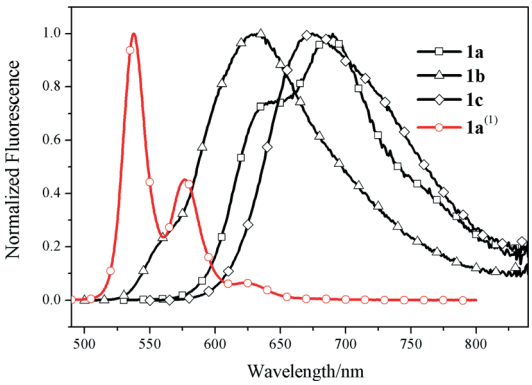

Fig. 7 Normalized fluorescence spectra of thin films of **1a–c**. (1) With monomeric **1a** (5.0×10^{-6} M in chloroform) as reference.

to the different absorption bands in the absorption spectrum. The presence of multiple emission bands in the fluorescence spectrum suggests that the molecules of **1a** in the solid films do not pack uniformly, but with different structures, which is consistent with the results of the absorption spectrum. The broad low energy emission of **1a** can be assigned to the "excimer-like" states.[69–71]

The maximum emission of **1b** can be found at about 633 nm, which is significantly blue shifted compared with that of **1a** in the solid state, but red-shifted compared with that of **1a** in solution. This is a typical emission of a slipped "face-to-face" stacked PDI dimer with longitudinal displacement.[63] This suggests that the molecules of **1b** in the solid state are stacked in a "face-to-face" way, but with longitudinal displacement between the nearby molecules, which corresponds well to the absorption spectra of **1b** in Fig. 1. The maximum emission wavelength of **1c** is about 680 nm, which is 50 nm longer than that of **1b**. According to the literature,[69–71] this emission can be assigned to the "excimer-like" states.

The absolute fluorescence quantum yields of these compounds are also measured and the results are summarized in Table 2. For compound series **1a–c**, **1a** presents the smallest solid state fluorescence quantum yield, which is understandable because of the smallest groups attached to it and the molecules of **1a** can approach each other without steric hindrance. **1b** has the largest solid state fluorescence quantum yield among these three compounds, which is unexpected because the flexible linkage between the POSS groups and the PDI core would make the molecules of **1b** more flexible and then less steric hindrance when two **1b** molecules come close to each other. This will leave a short distance between the molecules of **1b** and principally a strong interaction between the PDI molecules. However, the shorter wavelength emission together with the absorption character of **1b** suggests that it formed a slipped "face-to-face" stacked structure with longitudinal displacement in the solid state, while **1c** formed "H" type aggregates in the solid state without any indication of the presence of longitudinal displacement.[63] This is the reason why the solid state fluorescence quantum yield of **1b** is larger than that of **1c**.

The normalized fluorescence spectra of **2a–c** in the solid state are shown in the ESI† Fig. S2(a). All these three compounds show similar broad emission bands in the long wavelength region (660–680 nm), which can be assigned to the "excimer-like" states,[63] a typical feature of "face-to-face" stacked PDI molecules.[63,72] Due to the packing structures of these molecules in the solid state being different from each other, the maximum emission wavelengths vary from 660 nm for **2b** to 680 nm for **2a** and **2c**.[41,63,72]

Among these three compounds, **2b** presents the smallest solid state fluorescence quantum yield, while the solid state fluorescence quantum yields of **2a** and **2c** are almost the same. Obviously, the bulky POSS group of **2b** and **2c** did not promote the solid state fluorescence quantum yields as expected. This can be attributed to the different packing structures of the molecules in the solid state. **2a** and **2c** formed "J-type" aggregates as indicated by the red-shifted absorption bands,[63] while **2b** formed "H" aggregates as revealed by the blue-shifted absorption maximum. These results tell us again that the most important factor in determining the solid state fluorescence quantum yields of **2a–c** is the packing structure of the molecules in the solid state.

The solid state fluorescence spectra of **3a–c** are shown in the ESI† Fig. S2(b). The fluorescence spectra of these three compounds in the solid state are similar to each other. The emission peaks of these three compounds shifted to a longer wavelength compared with those of **3a** in solution, which can be attributed the interactions between the molecules. The absolute fluorescence quantum yields of **3a** and **3b** are similar to each other, which means that the POSS groups in **3b** do not benefit the solid state fluorescence quantum yield. However, the solid state fluorescence quantum yield of **3c** is significantly larger than those of **3a** and **3b**. As revealed by the red shift of the absorption bands with respect to that in solution and the crystal structure of these compounds, all these three compounds formed "J" type aggregates in the solid state. But the red-shifts of **3a** and **3b** are almost identical, which means that the interaction intensity between the neighbour molecules is the same. However, the red-shifts of the absorption bands of **3c** are significantly smaller than those of **3a** and **3b**, which means that the intensity of the interactions between the neighbour molecules of **3c** is small, and thus the solid state fluorescence quantum yield of **3c** is larger than those of **3a** and **3b**.

By comparing the solid state fluorescence quantum yields of **1a**, **2a** and **3a**, we can conclude that the bay substituents can improve the solid state emission properties to some extent. However, the effects of bay substituents on the promotion of the solid state fluorescence quantum yields of other two compound series (**1b**, **2b**, **3b** and **1c**, **2c**, **3c**) are not so significant. Compounds **1b** and **3c** are the best two solid state emitters among these nine compounds. This result indicates that the introduction of bulky groups into a molecule will not inevitably lead to a significant improvement in the emission properties. The crucial factor, which affects the solid state emission properties, is the packing structure of the molecules in the solid state. Avoiding the formation of "H" type aggregates in the solid state seems to be a rational strategy towards a good solid state emitter.

Conclusions

Three series of PDI compounds equipped with POSS groups *via* flexible or rigid linkages have been synthesized to clarify the synergistic effect of substituents at the bay positions and POSS groups at imide nitrogen on the reduction of the aggregation of PDI molecules in the solid state. The POSS groups at the imide nitrogen bring about large changes in the packing structure of the molecules in the solid state. Based on the changes in the solid state absorption spectra against those in solution, the packing structures of the molecules in the solid state are proposed and three of them have been verified by the crystal structure. Most of the molecules are packed in a "face-to-face" way, but with different longitudinal displacement. Large longitudinal displacement leads to "J" type interactions between the neighbour molecules in the solid state and large solid state fluorescence quantum yields, while the small longitudinal displacement causes "H" type interactions and small solid state fluorescence quantum yields. The packing structure of the molecules in the solid state is the dominating factor in determining the solid state fluorescence quantum yields. The introduction of bulky groups in PDI molecules will not inevitably promote the solid state fluorescence quantum yields.

Acknowledgements

We thank the Natural Science Foundation of China (grand no. 21173136 and 91233108), the National Basic Research Program of China (973 Program: 012CB93280) and Shandong University for financial support.

Notes and references

1 J. Mei, Y. Diao, A. L. Appleton, L. Fang and Z. Bao, *J. Am. Chem. Soc.*, 2013, **135**, 6724–6746.
2 C. R. Newman, C. D. Frisbie, D. A. da Silva, J. L. Bredas, P. C. Ewbank and K. R. Mann, *Chem. Mater.*, 2004, **16**, 4436–4451.
3 B. A. Jones, M. J. Ahrens, M. H. Yoon, A. Facchetti, T. J. Marks and M. R. Wasielewski, *Angew. Chem., Int. Ed.*, 2004, **43**, 6363–6366.
4 P. Ranke, I. Bleyl, J. Simmerer, D. Haarer, A. Bacher and H. W. Schmidt, *Appl. Phys. Lett.*, 1997, **71**, 1332–1334.
5 M. A. Angadi, D. Gosztola and M. R. Wasielewski, *Mater. Sci. Eng., B*, 1999, **63**, 191–194.
6 S. Alibert-Fouet, S. Dardel, H. Bock, M. Oukachmih, S. Archambeau, I. Seguy, P. Jolinat and P. Destruel, *ChemPhysChem*, 2003, **4**, 983–985.
7 P. Schouwink, A. H. Schäfer, C. Seidel and H. Fuchs, *Thin Solid Films*, 2000, **372**, 163–168.
8 T. Zukawa, S. Naka, H. Okada and H. Onnagawa, *J. Appl. Phys.*, 2002, **91**, 1171–1174.

9 J.-S. Heo, N.-H. Park, J.-H. Ryu and K.-D. Suh, *Adv. Mater.*, 2005, **17**, 822–826.
10 C. Ego, D. Marsitzky, S. Becker, J. Zhang, A. C. Grimsdale, K. Müllen, J. D. MacKenzie, C. Silva and R. H. Friend, *J. Am. Chem. Soc.*, 2003, **125**, 437–443.
11 Y. Tani, T. Seki, X. Lin, H. Kurata, S. Yagai and K. Nakayama, *Mol. Cryst. Liq. Cryst.*, 2013, **578**, 88–94.
12 J. Hua, F. Meng, F. Ding, F. Li and H. Tian, *J. Mater. Chem.*, 2004, **14**, 1849–1853.
13 F. G. Brunetti, R. Kumar and F. Wudl, *J. Mater. Chem.*, 2010, **20**, 2934–2948.
14 B. A. Gregg, *J. Phys. Chem. B*, 2003, **107**, 4688–4698.
15 C. Huang, S. Barlow and S. R. Marder, *J. Org. Chem.*, 2011, **76**, 2386–2407.
16 M. J. Ahrens, M. J. Tauber and M. R. Wasielewski, *J. Org. Chem.*, 2006, **71**, 2107–2114.
17 J. Vura-Weis, M. A. Ratner and M. R. Wasielewski, *J. Am. Chem. Soc.*, 2010, **132**, 1738–1739.
18 C. Zhao, Y. Zhang, R. Li, X. Li and J. Jiang, *J. Org. Chem.*, 2007, **72**, 2402–2410.
19 C.-C. Chao, M.-k. Leung, Y. O. Su, K.-Y. Chiu, T.-H. Lin, S.-J. Shieh and S.-C. Lin, *J. Org. Chem.*, 2005, **70**, 4323–4331.
20 A. J. Jimenez, M.-J. Lin, C. Burschka, J. Becker, V. Settels, B. Engels and F. Würthner, *Chem. Sci.*, 2014, **5**, 608–619.
21 S. W. Eaton, L. E. Shoer, S. D. Karlen, S. M. Dyar, E. A. Margulies, B. S. Veldkamp, C. Ramanan, D. A. Hartzler, S. Savikhin, T. J. Marks and M. R. Wasielewski, *J. Am. Chem. Soc.*, 2013, **135**, 14701–14712.
22 H. Langhals, O. Krotz, K. Polborn and P. Myer, *Angew. Chem., Int. Ed.*, 2005, **44**, 2427–2428.
23 H. Langhals, R. Ismael and O. Yürük, *Tetrahedron*, 2000, **56**, 5435–5441.
24 Y. Liu, K.-R. Wang, D.-S. Guo and B.-P. Jiang, *Adv. Funct. Mater.*, 2009, **19**, 2230–2235.
25 J. Feng, B. Liang, D. Wang, H. Wu, L. Xue and X. Li, *Langmuir*, 2008, **24**, 11209–11215.
26 T. Heek, C. Fasting, C. Rest, X. Zhang, F. Würthner and R. Haag, *Chem. Commun.*, 2010, **46**, 1884–1886.
27 C. D. Schmidt, C. Böttcher and A. Hirsch, *Eur. J. Org. Chem.*, 2007, **33**, 5497–5505.
28 M. Tanahashi, *Materials*, 2010, **3**, 1593–1619.
29 J. D. Lichtenhan, Y. A. Otonari and M. J. Carr, *Macromolecules*, 1995, **28**, 8435–8437.
30 L. Marta, P.-S. Mercedes, A.-G. Francisco and S. Roberto, *J. Mater. Chem.*, 2011, **21**, 12803–12811.
31 B. Trastoy, M. E. Pérez-Ojeda, R. Sastre and J. L. Chiara, *Chem. – Eur. J.*, 2010, **16**, 3833–3841.
32 J. Sun, Y. Chen, L. Zhao, Y. Chen, D. Qi, K.-M. Choi, D.-S. Shin and J. Jiang, *Chem. – Eur. J.*, 2013, **19**, 12613–12618.
33 T. Ceyhan, A. Altindal, A. R. Özkaya, B. Salihd and Ö. Bekaroğlu, *Dalton Trans.*, 2009, 10318–10329.
34 J. Zhou, Y. C. Zhao, K. Yu, X. Zhou and X. Xie, *New J. Chem.*, 2011, **35**, 2781–2792.
35 P. A. Ledin, I. M. Tkachenko, W. Xu, I. Choi, V. V. Shevchenko and V. V. Tsukruk, *Langmuir*, 2014, **30**, 8856–8865.
36 F. Du, Y. Bao, B. Liu, J. Tian, Q. Li and R. Bai, *Chem. Commun.*, 2013, **49**, 4631–4633.
37 G. M. Sheldrick, *SHELXS-97, Program for X-ray Crystal Structure Determination*, University of Göttingen, Germany, 1997.
38 G. M. Sheldrick, *SHELXL-97, Program for X-ray Crystal Structure Refinement*, University of Göttingen, Germany, 1997.
39 C. Suspene and J.-P. Simonato, *US Pat.* Appl., US 2012/0116084 A1, 2010.
40 X. K. Ren, B. Sun, C. C. Tsai, Y. F. Tu, S. W. Leng, K. X. Li, Z. Kang, R. M. Van Horn, X. P. Li, M. F. Zhu, C. Wesdemiotis, W. B. Zhang and S. Z. D. Cheng, *J. Phys. Chem. B*, 2010, **114**, 4802–4810.
41 J. Feng, Y. Zhang, C. Zhao, R. Li, W. Xu, X. Li and J. Jiang, *Chem. – Eur. J.*, 2008, **14**, 7000–7010.
42 S. W. Leng, B. Wex, L. H. Chan, M. J. Graham, S. Jin, A. J. Jing, K. U. Jeong, R. M. Van Horn, B. Sun, M. F. Zhu, B. R. Kaafarani and S. Z. D. Cheng, *J. Phys. Chem. B*, 2009, **113**, 5403–5411.
43 S. W. Leng, L. H. Chan, J. Jing, J. Hu, R. M. Moustafa, R. M. Van Horn, M. J. Graham, B. Sun, M. F. Zhu, K. U. Jeong, B. R. Kaafarani, W. B. Zhang, F. W. Harris and S. Z. D. Cheng, *Soft Matter*, 2010, **6**, 100–112.
44 G. Li, L. Wang, H. Ni and C. U. Pittman Jr, *J. Inorg. Organomet. Polym.*, 2001, **11**, 123–154.
45 S. Xiao, M. Nguyen, X. Gong, Y. Cao, H. B. Wu, D. Moses and A. J. Heeger, *Adv. Funct. Mater.*, 2003, **13**, 25–29.
46 L. Cui, J. P. Collet, G. Q. Xu and L. Zhu, *Chem. Mater.*, 2006, **18**, 3503–3512.
47 F. Würthner, Z. J. Chen, V. Dehm and V. Stepanenko, *Chem. Commun.*, 2006, 1188–1190.
48 L. Zhao, T. Ma, H. Bai, G. Lu, C. Li and G. Q. Shi, *Langmuir*, 2008, **24**, 4380–4387.
49 V. J. Sapagovas, V. Gaidelis, V. Kovalevskij and A. Undzenas, *Dyes Pigm.*, 2006, **71**, 178–187.
50 H. Langhals, S. Demmig and H. Huber, *Spectrochim. Acta, Part A*, 1988, **44**, 1189.
51 H. Langhals, *Helv. Chim. Acta*, 2005, **88**, 1309–1343.
52 E. M. Calzado, J. M. Villalvilla, P. G. Boj, J. A. Quintana, R. Gómez, J. L. Segura and M. A. Díaz-García, *J. Phys. Chem. C*, 2007, **111**, 13595–13605.
53 K. Sugiyasu, N. Fujita and S. Shinkai, *Angew. Chem., Int. Ed.*, 2004, **43**, 1229–1233.
54 C. Kohl, T. Weil, J. Qu and K. Müllen, *Chem. – Eur. J.*, 2004, **10**, 5297–5310.
55 P. Osswald, D. Leusser, D. Stalke and F. Würthner, *Angew. Chem., Int. Ed.*, 2005, **44**, 250–253.
56 Z. Chen, M. G. Debije, T. Debaerdemaeker, P. Osswald and F. Würthner, *ChemPhysChem*, 2004, **5**, 137–140.
57 E. K. Theo, W. Hao, S. Vladimir and F. Würthner, *Angew. Chem., Int. Ed.*, 2007, **46**, 5541–5544.
58 P. M. Kazmaier and R. Hoffmann, *J. Am. Chem. Soc.*, 1994, **116**, 9684–9691.
59 J. M. Giaimo, J. V. Lockard, L. E. Sinks, A. M. Scott, T. M. Wilson and M. R. Wasielewski, *J. Phys. Chem. A*, 2008, **112**, 2322–2330.

60 W. Wang, L.-S. Li, G. Helms, H.-H. Zhou and A. D. Q. Li, *J. Am. Chem. Soc.*, 2003, **125**, 1120–1121.
61 K. Balakrishnan, A. Datar, R. Oitker, H. Chen, J. Zuo and L. Zang, *J. Am. Chem. Soc.*, 2005, **127**, 10496–10497.
62 K. Balakrishnan, A. Datar, T. Naddo, J. Huang, R. Oitker, M. Yen, J. Zhao and L. Zang, *J. Am. Chem. Soc.*, 2006, **128**, 7390–7398.
63 H. Liu, L. Shen, Z. Cao and X. Li, *Phys. Chem. Chem. Phys.*, 2014, **16**, 16399–16406.
64 J. M. Giaimo, A. V. Gusev and M. R. Wasielewski, *J. Am. Chem. Soc.*, 2002, **124**, 8530–8531.
65 Z. J. Chen, V. Stepanenko, V. Dehm, P. Prins, L. D. A. Siebbeles, J. Seibt, P. Marquetand, V. Engel and F. Würthner, *Chem. – Eur. J.*, 2007, **13**, 436–449.
66 F. Würthner, Z. J. Chen, F. J. M. Hoeben, P. Osswald, C. C. You, P. Jonkheijm, J. von Herrikhuyzen, A. P. H. J. Schenning, P. P. A. M. van der Schoot, E. W. Meijer, E. H. A. Beckers, S. C. J. Meskers and R. A. J. Janssen, *J. Am. Chem. Soc.*, 2004, **126**, 10611–10618.
67 D. Clarke, S. Mathewb, J. Matisons, G. Simon and B. W. Skelton, *Dyes Pigm.*, 2011, **92**, 659–667.
68 Z. J. Chen, U. Baumeister, C. Tschierske and F. Würthner, *Chem. – Eur. J.*, 2007, **13**, 450–465.
69 J. M. McCrate and J. G. Ekerdt, *J. Phys. Chem. C*, 2014, **118**, 2104–2114.
70 A. M. Ara, T. Iimori, T. Yoshizawa, T. Nakabayashi and N. Ohta, *Chem. Phys. Lett.*, 2006, **427**, 322–328.
71 K. E. Brown, W. A. Salamant, L. E. Shoer, R. M. Young and M. R. Wasielewski, *J. Phys. Chem. Lett.*, 2014, **5**, 2588–2593.
72 T. V. D. Boom, R. T. Hayes, Y. Y. Zhao, P. J. Bushard, E. A. Weiss and M. R. Wasielewski, *J. Am. Chem. Soc.*, 2002, **124**, 9582–9590.